Molecular Physics, Vol. 105, Nos. 2–3, 20 January–10 February 2007, 261–272

Molecular simulation and theoretical modeling of polyhedral oligomeric silsesquioxanes

Y. PENG and C. McCABE*
Vanderbilt University, Nashville, USA

(*Received 15 June 2006; in final form 28 October 2006*)

Polyhedral oligomeric silsesquioxane (POSS) molecules are unique nanometre-size inorganic/organic hybrid structures based on a $(SiO_{1.5})_8$ core. Depending on the functionalization of the POSS cages, the resulting systems can be solid or liquid, or, upon crosslinking, turned into a network. While much is known experimentally about the chemical synthesis of POSS systems, very little theoretical understanding exists at the molecular level or beyond. Of particular interest is the study of the effect of tether groups on the thermodynamic properties and phase behaviour of POSS fluids, which is addressed in this work through both molecular simulation and the statistical associating fluid theory for potentials of variable attractive range (SAFT-VR). In this application of SAFT-VR to POSS molecules the hetero-SAFT-VR approach is used. The POSS cage is represented as a single sphere and the tether groups by one or more smaller spheres, depending on chain length. Since very limited experimental data is available for the thermodynamic properties of POSS systems, molecular dynamics simulations are used to obtain pseudo-experimental data with which to validate the theoretical approach. Good agreement is obtained between the simulation data and the theoretical results and predictions are made for systems yet to be studied by simulation or experiment.

1. Introduction

Polyhedral oligomeric silsesquioxanes (POSS) molecules are unique nanometre-size inorganic/organic hybrid structures based on a $(SiO_{1.5})_8$ core. POSS can be functionalized with the same organic or inorganic group on each corner of the cube ($R_8Si_8O_{12}$) or with one group on one corner and a different group on the others ($RR'_7Si_8O_{12}$), the simplest POSS monomer being hydrogen terminated POSS ($H_8Si_8O_{12}$). The ability to synthesize POSS cubes with different functional groups results in a large number of possible POSS-based molecules whose physical properties can be tailored through manipulation of the functional groups, opening up many possible application areas for POSS-based materials [1].

POSS molecules can either be physically blended with polymers to form nanocomposite materials or chemically grafted to polymeric chains, where they form a crosslinked polymer network or serve as pendant groups on the polymer backbone. The incorporation of POSS molecules into polymeric materials often results in dramatic improvements in the material properties such as oxidation resistance, surface hardening, improved mechanical and thermal properties and reductions in flammability and heat evolution [2]. The properties of POSS–polymer blends depend on the interactions between the POSS molecules and the polymer. For example, untethered cyclohexyl- and isobutyl-POSS fillers, when well dispersed in polymethyl methacrylate (PMMA), decrease the zero-shear viscosity. However, once the solubility limit of the POSS molecular is reached, the untethered POSS aggregates into crystallites and leads to an increase in the viscosity [3]. In the same study, blends of POSS–PMMA copolymer with isobutyl-POSS were observed to show a dramatic increase in viscosity with the addition of even small amounts of POSS fillers due to the interactions between the free POSS and POSS pendants [3].

In recent years research on POSS based systems, particularly synthesis and structural properties, has increased significantly. Information on the thermodynamic properties, however, is more scarce. The melting points of 8-fold alkyl substituted POSS have been studied and show a sharp decrease from octa-propyl-POSS to octa-pentyl-POSS, while molecules with

*Corresponding author. Email: c.mccabe@vanderbilt.edu

Molecular Physics
ISSN 0026–8976 print/ISSN 1362–3028 online © 2007 Taylor & Francis
http://www.tandf.co.uk/journals
DOI: 10.1080/00268970701189244

longer alkyl chains (C_5–C_{10}) show an odd–even effect [4] similar to that observed for other homologous series [5]. From a theoretical point of view it is interesting to study both octa- and mono-substituted POSS systems with simple tether groups like the alkanes, as this allows a systematic study of the effect of the tether on the thermodynamic properties. Although such systems might be considered model compounds for silsesquioxane-based materials, they do show potentially interesting properties, including their use as amphiphiles for novel core/shell type silicate nanoparticles [6].

In order to obtain a better understanding of POSS systems at a molecular level, several simulation studies have recently appeared [7–16]. For example, using a minimal model to mimic POSS systems, Lamm and co-workers [8] studied the structural properties of cross-linked POSS networks using lattice Monte Carlo simulations. The effect of the length of the linkers between POSS cages on network structural properties was examined and the porosity was seen to decrease with increasing tether length, in agreement with experimental data. In work closer to the current study, a number of atomistic molecular dynamics simulations have been performed on POSS–solvent and POSS–polymer systems [7, 10–13]. In particular, Striolo and co-workers [11, 12, 16, 17] studied dilute solutions of hydrogen-terminated and octa-substituted POSS monomers in poly(dimethylsiloxane), n-hexadecane and n-hexane to probe the POSS–solvent interactions. This work illustrated that it is possible to modulate the effective POSS–POSS interaction by increasing the temperature, solvent and/or functional groups on the POSS cage.

Although molecular simulation is a useful tool with which to study atomic and nano-scale processes, a theoretical approach can much more rapidly study a wide range of systems than is possible by simulation. There are many theoretical approaches available to describe the thermodynamics and physical properties of fluid systems. However, in contrast to traditional equations such as activity coefficient models and cubic equations of state (EOS), molecular-based approaches provide the opportunity to develop a molecular-level basis for the observed behaviour and a more predictive approach. In particular, the molecular-based SAFT approach [18, 19] provides a framework in which the effects of molecular shape and interactions on the thermodynamic properties can be separated and quantified. The explicit description of the molecular-level interactions enables the parameters of the resulting equation of state to have physical meaning, leading to more predictive capabilities and a limited reliance on fitting to experimental data. While there are several versions of the SAFT equation available [20, 21], we focus on the SAFT-VR [22, 23] equation in which monomers interact through a potential of variable attractive range (VR). The SAFT-VR equation has been successfully used to describe the phase equilibria of a wide range of industrially important systems, from alkanes of low molecular weight to simple polymers [24–26] and electrolyte solutions [27–29], and has recently been extended to accurately model the critical region [30–32] and rigorously incorporate dipolar interactions into the model chain [33]. In this work, we apply the hetero-SAFT-VR approach developed by McCabe and co-workers [34, 35] to study the effect of tether groups on the thermodynamic properties of both mono-tethered and homogeneously multi-tethered POSS molecules. The theoretical method is described in section 2 and details of the molecular dynamics simulations performed to parameterize and validate the theoretical model are given in section 3. The theoretical results are presented and compared with molecular simulations in section 4 and conclusions drawn and future work discussed in section 5.

2. Hetero-SAFT-VR approach

In the SAFT-VR approach molecules are modelled as chains of tangentially bonded hard-sphere segments that interact through an attractive potential of variable range. In this approach each segment in the model chain has the same size and energy parameters. The hetero-SAFT-VR approach allows molecules to be described as chains of tangentially bonded segments that can have different size and/or energy parameters. In earlier work we validated the hetero-SAFT-VR approach using isothermal-isobaric (NPT) and Gibbs ensemble Monte Carlo (GEMC) simulation data and demonstrated that the theory can accurately capture the effects of interaction energy, segment size and molecular structure on the PVT and phase behaviour of hetero-nuclear diblock fluids [35]. In the same spirit, the hetero-SAFT-VR approach allows us to model alkyl-tethered POSS molecules as a single spherical POSS core connected to a number of smaller segments that describe the alkyl tethers as shown in figure 1(b). Each segment in the model interacts through a square well (SW) potential,

$$U_{ij}(r) = \begin{cases} +\infty & \text{if} \quad r < \sigma_{ij} \\ -\varepsilon_{ij} & \text{if} \quad \sigma_{ij} \le r < \lambda_{ij}\sigma_{ij} \\ 0 & \text{if} \quad r \ge \lambda_{ij}\sigma_{ij} \end{cases} \tag{1}$$

where σ_{ij} is the diameter of the interaction, λ_{ij} the range and ε_{ij} the well depth of the SW potential. The inter- and intra-molecular cross-interactions between segments are

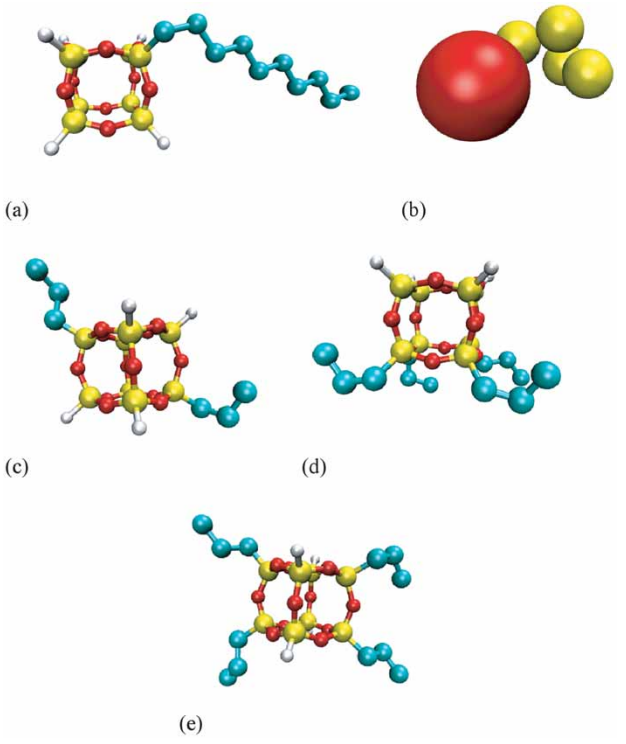

Figure 1. Schematic illustration of (a) mono-tethered decyl-POSS; (b) the hetero-SAFT-VR model for mono-tethered decyl-POSS; (c) di-tethered propyl-POSS; and (d) and (e) the two different tetra-tethered propyl-POSS molecules studied.

obtained from the Lorentz–Berthelot combining rules [36]:

$$\sigma_{ij} = \frac{\sigma_{ii} + \sigma_{jj}}{2} \tag{2}$$

$$\varepsilon_{ij} = \sqrt{\varepsilon_{ii}\,\varepsilon_{jj}} \tag{3}$$

$$\lambda_{ij} = \frac{\lambda_{ii}\,\sigma_{ii} + \lambda_{jj}\,\sigma_{jj}}{\sigma_{ii} + \sigma_{jj}}. \tag{4}$$

In the hetero-SAFT-VR approach the Helmholtz free energy A takes the same general form as in the original SAFT formalism, namely

$$\frac{A}{NkT} = \frac{A^{ideal}}{NkT} + \frac{A^{mono}}{NkT} + \frac{A^{chain}}{NkT} + \frac{A^{assoc}}{NkT} \tag{5}$$

where A^{ideal} is the ideal contribution to the free energy, A^{mono} the contribution due to the monomer segments, A^{chain} the contribution due to chain formation from the monomer segments, and A^{assoc} the contribution due to association interactions, which we do not consider in this work. In the hetero-SAFT-VR, equation (5) describes the free energy of a hetero-segmented pure fluid that is composed of segments of two different kinds. Here, we briefly describe the main expressions of the hetero-SAFT-VR approach and refer the reader to the original papers for additional details [34, 35].

The ideal contribution to the free energy is given by

$$\frac{A^{ideal}}{NkT} = \ln(\rho\Lambda^3) - 1 \tag{6}$$

where N is the total number of molecules, k Boltzmann's constant, ρ the number density of chain molecules and Λ the thermal de Broglie wavelength.

The monomer free energy is expressed as

$$\frac{A^{mono}}{NkT} = m\frac{A^{M}}{N_s kT} = ma^{M} \tag{7}$$

where N_s is the total number of segments and m the number of segments per molecule. a^M is free energy per monomer segment and is approximated by the Barker–Henderson second-order high temperature expansion [37], namely

$$a^{M} = a^{HS} + \beta a_1 + \beta^2 a_2 \tag{8}$$

where $\beta = 1/kT$, a^{HS} is the free energy of the hard sphere reference fluid and a_1 and a_2 are the first and second perturbation terms, respectively.

The hard sphere reference term a^{HS} is determined from the expression of Boublik [38] and Mansoori and co-workers [39] for multicomponent hard sphere systems, namely

$$a^{HS} = \frac{6}{\pi\rho_s}\left[\left(\frac{\zeta_2^3}{\zeta_3^2} - \zeta_0\right)\ln(1-\zeta_3) + \frac{3\zeta_1\zeta_2}{1-\zeta_3} + \frac{\zeta_2^3}{\zeta_3(1-\zeta_3)^2}\right] \tag{9}$$

where ρ_s is the number density of segments and ζ_l the reduced density given by a sum over all segments i

$$\zeta_l = \frac{\pi}{6}\rho_s\left[\sum_{i=1}^{n} x_{s,i}(\sigma_i)^l\right] \tag{10}$$

with σ_i the diameter of segments of type i and $x_{s,i}$ the mole fraction of segments of type i. Note ζ_3 is the volume fraction occupied by the molecules and is generally denoted as η.

The first perturbation term a_1, which describes the mean-attractive energy, is obtained from the sum of all pair interactions:

$$\begin{aligned} a_1 &= \sum_{i=1}^{n}\sum_{j=1}^{n} x_{s,i}\,x_{s,j}(a_1)_{ij} \\ &= x_{s,1}^2(a_1)_{11} + 2x_{s,1}\,x_{s,2}(a_1)_{12} + x_{s,2}^2(a_1)_{22} \end{aligned} \tag{11}$$

where $(a_1)_{ij}$ is obtained from the mean-value theorem as proposed by Gil-Villegas *et al*. [22]:

$$(a_1)_{ij} = -2\pi\rho_s\varepsilon_{ij}\int_{\sigma_{ij}}^{\infty} r_{ij}^2 g_{ij}^{HS}(r_{ij})dr_{ij} = -\rho_s\frac{2\pi}{3}\sigma_{ij}^3\varepsilon_{ij}\left(\lambda_{ij}^3-1\right)g_{ij}^{HS}\left(\sigma_{ij};\zeta_3^{eff}\right). \quad (12)$$

Equation (12) can be simplified within the van der Waals one fluid theory to

$$(a_1)_{ij} = -\rho_s\frac{2\pi}{3}\sigma_{ij}^3\varepsilon_{ij}\left(\lambda_{ij}^3-1\right)g_0^{HS}\left[\sigma_x;\zeta_x^{eff}(\lambda_{ij})\right] \quad (13)$$

where $g_0^{HS}(\sigma_x;\zeta_x^{eff})$ is obtained from the Carnahan and Starling equation of state for pure fluids [40]:

$$g_0^{HS}\left[\sigma_x;\zeta_x^{eff}(\lambda_{ij})\right] = \frac{1-\zeta_x^{eff}/2}{\left(1-\zeta_x^{eff}\right)^3}. \quad (14)$$

The effective packing fraction $\zeta_x^{eff}(\lambda_{ij})$ is obtained within the van der Waals one fluid theory from the corresponding packing fraction of the mixture ζ_x and is given by

$$\zeta_x^{eff}(\zeta_x,\lambda_{ij}) = c_1(\lambda_{ij})\zeta_x + c_2(\lambda_{ij})\zeta_x^2 + c_3(\lambda_{ij})\zeta_x^3 \quad (15)$$

where

$$\begin{pmatrix} c_1 \\ c_2 \\ c_3 \end{pmatrix} = \begin{pmatrix} 2.25855 & -1.50349 & 0.249434 \\ -0.669270 & 1.40049 & -0.827739 \\ 10.1576 & -15.0427 & 5.30827 \end{pmatrix}\begin{pmatrix} 1 \\ \lambda_{ij} \\ \lambda_{ij}^2 \end{pmatrix} \quad (16)$$

and

$$\zeta_x = \frac{\pi}{6}\rho_s\sigma_x^3 = \frac{\pi}{6}\rho_s\sum_{i=1}^{n}\sum_{j=1}^{n}x_{s,i}\,x_{s,j}\,\sigma_{ij}^3 = \frac{\pi}{6}\rho_s\left(x_{s,1}^2\sigma_{11}^3 + 2x_{s,1}\,x_{s,2}\sigma_{12}^3 + x_{s,2}^2\sigma_{22}^3\right). \quad (17)$$

This corresponds to mixing rule MX1b in the original SAFT-VR approach for mixtures [23].

The second-order perturbation term a_2, is expressed as

$$a_2 = \sum_{i=1}^{n}\sum_{j=1}^{n}x_{s,i}\,x_{s,j}\,(a_2)_{ij} = x_{s,1}^2(a_2)_{11} + 2x_{s,1}x_{s,2}\,(a_2)_{12} + x_{s,2}^2(a_2)_{22} \quad (18)$$

where $(a_2)_{ij}$ is determined from the local compressibility approximation:

$$(a_2)_{ij} = \frac{1}{2}K^{HS}\,\varepsilon_{ij}\rho_s\frac{\partial(a_1)_{ij}}{\partial\rho_s} \quad (19)$$

and K^{HS} is the Percus–Yevick expression for the hard-sphere isothermal compressibility.

Finally, the contribution due to chain formation from the monomer segments is given in terms of the background correlation function y_{ij}^{SW},

$$\frac{A^{chain}}{NkT} = -\sum_{ij\ \text{bonds}}\ln y_{ij}^{SW}(\sigma_{ij}) \quad (20)$$

where the sum is over all bonds in the chain molecule and in this work becomes

$$\frac{A^{chain}}{NkT} = -N_t\left[\ln y_{12}^{SW}(\sigma_{12}) + (m_2-1)\ln y_{22}^{SW}(\sigma_{22})\right]. \quad (21)$$

Here, N_t is the number of tethers per molecule and m_2 is the number of alkyl segments per tether. The background correlation function is given by

$$y_{ij}^{SW}(\sigma_{ij}) = \exp(-\beta\varepsilon_{ij})g_{ij}^{SW}(\sigma_{ij}) \quad (22)$$

and the radial distribution function for the square well monomers $g_{ij}^{SW}(\sigma_{ij})$ is approximated by a first-order high-temperature perturbation expansion:

$$g_{ij}^{SW}(\sigma_{ij};\zeta_3) = g_{ij}^{HS}(\sigma_{ij};\zeta_3) + \beta\varepsilon_{ij}\,g_1^{SW}(\sigma_{ij}) \quad (23)$$

where the contact value of the radial distribution function $g_{ij}^{HS}(\sigma_{ij};\zeta_3)$ at the actual packing fraction ζ_3 is obtained from the expression of Boublik [38] and $g_1^{SW}(\sigma_{ij})$ is determined from the Clausius virial theorem and the first derivative of the free energy with respect to the density [22].

Thermodynamic properties such as pressure and chemical potential can now be calculated from the Helmholtz free energy through standard thermodynamic relationships:

$$P = -\left(\frac{\partial A}{\partial V}\right)_{T,N} \quad (24)$$

$$\mu = \left(\frac{\partial A}{\partial N_i}\right)_{T,V,N_{j\neq i}} \quad (25)$$

3. Simulation details

In order to study POSS molecules with the hetero-SAFT-VR approach the theoretical model parameters (i.e. $m, \sigma, \varepsilon, \lambda$) for the POSS cube must be determined. Typically the SAFT parameters are obtained by fitting to experimental thermodynamic property data. However, the dearth of experimental data on the thermodynamics of POSS-based molecules makes it very difficult to calibrate the hetero-SAFT-VR model by comparison with experiment. Hence, here we calibrate the theory using simulation data based on reliable force fields. This can be thought of as a coarse-graining of the atomistic simulation, albeit into a coarse-grained theoretical model, as opposed to the usual coarse-grained force field model. Molecular dynamics simulations were performed for seven different mono- and multi-tethered POSS fluids: mono-tethered propyl-, hexyl- and, nonyl- POSS; di-tethered propyl-POSS, tetra-tethered propyl-POSS with two different arrangements of the tethers on the POSS cube, and octa-tethered propyl-POSS (as shown in figure 1).

The molecular dynamics simulations were carried out using the DL_POLY 2 simulation software [41] with atomistic force fields for the POSS and tether molecules as described below. Simulations were performed in the canonical (NVT) ensemble using the Berendsen thermostat [42] to maintain the temperature. In each simulation 64 POSS molecules (ranging from 1920 atoms to 2816 atoms) were used and the usual periodic boundary conditions were applied to the simulation box. Initially simulations were also performed with 128 POSS molecules; however, no difference was observed in the calculated density and so 64 molecules were used for all production runs. A time step of 1 fs was employed and a cutoff of 10 Å used for non-bonded interactions. Each simulation was started from a lattice configuration and then equilibrated for 100 ps, followed by production runs of 400–500 ps during which the properties of interest were calculated. For each system three isotherms were studied (700 K, 900 K and 1200 K) and the pressure profile obtained for a series of densities between $\eta = 0.1$ and 0.45. The temperatures were chosen to ensure the POSS systems were above the experimental and force field melting points [43]. While POSS monomers probably decompose at 1000 K [44], the high temperature results correspond to hypothetical results that would be obtained in the absence of decomposition. From the point of view of determining effective parameters for use in a hetero-SAFT-VR model, the absence of decomposition in either the simulation or the hetero-SAFT-VR models is not a drawback; our goal here is to calibrate the molecular model using simulation data. A similar problem existed in the calibration of alkane force fields against experimental phase equilibrium and critical point data [45], as such models also do not include decomposition.

The Hybrid-COMPASS (HC) force field [46, 47] was used to describe the POSS molecules. The HC force field was shown in earlier work to be successful in describing the structural properties of POSS systems [43]. The TraPPE united atom model [48], which was specifically developed to study the fluid phase behaviour of alkanes, was used to describe the alkyl tethers. *Ab initio* calculations of alkyl-tethered POSS systems [49] have shown that the POSS cage is not significantly influenced by the tether and vice versa, indicating that it is possible to combine force fields developed independently to study functionalized POSS systems and take advantage of specifically developed force fields for the tethered groups. Below we briefly describe the force fields used.

3.1. *POSS cube*

As in earlier work [43] the simplified or hybrid COMPASS force field was used to model the POSS cube. In this model bond stretching U_b, bond angle-bending U_θ and torsional motion U_ϕ are respectively described by:

$$U_b = k_2(b-b_0)^2 + k_3(b-b_0)^3 + k_4(b-b_0)^4 \quad (26)$$

$$U_\theta = H_2(\theta-\theta_0)^2 + H_3(\theta-\theta_0)^3 + H_4(\theta-\theta_0)^4 \quad (27)$$

$$U_\Phi = V_1(1-\cos(\Phi)) + V_2(1-\cos(2\Phi)) + V_3(1-\cos(3\Phi)) \quad (28)$$

where b, θ, and Φ are the bond length, bond angle, and dihedral angle, respectively, b_0 the equilibrium bond length, θ_0 the equilibrium bond angle and $k_2, k_3, k_4, H_2, H_3, H_4$, and V_1, V_2, V_3 constants.

Nonbonded interactions are described by a Lennard–Jones 9–6 function:

$$U_{vdw} = \varepsilon_{ij}\left[2\left(\frac{\sigma_{ij}}{r}\right)^9 - 3\left(\frac{\sigma_{ij}}{r}\right)^6\right]. \quad (29)$$

The cross-interaction parameters σ_{ij} and ε_{ij} are calculated using a 6th-order combining rule:

$$\sigma_{ij} = \left(\frac{\sigma_i^6 + \sigma_j^6}{2}\right)^{1/6} \quad (30)$$

$$\varepsilon_{ij} = \left(\frac{2\sigma_i^3\,\sigma_j^3\sqrt{\varepsilon_i\,\varepsilon_j}}{\sigma_i^6 + \sigma_j^6}\right) \quad (31)$$

where σ_i, σ_j, ε_i, ε_j are the interaction parameters for the like atoms. Details of the potential model parameters used for the hybrid-COMPASS force field are reported in table 1.

3.2. *Alkyl tethers*

The alkyl tethers are described using the TraPPE united-atom force field [48] for alkanes in which each carbon atom and its bonded hydrogen atoms are treated as a single spherical interaction site. Bond-stretching U_b and bond-angle-bending U_θ terms are described by simple harmonic functions:

$$U_b = \frac{1}{2}k_{ij}(r - r_{ij})^2 \tag{32}$$

$$U_\theta = \frac{1}{2}k_\theta(\theta - \theta_0)^2 \tag{33}$$

where k_{ij} and k_θ are the force constants, r_{ij} is the equilibrium bond length between atoms i and j and θ_0 is the equilibrium angle. The torsion potential is expressed as a cosine function:

$$U_\Phi = c_1[1 + \cos(\Phi)] + c_2[1 - \cos(2\Phi)] + c_3[1 + \cos(3\Phi)] \tag{34}$$

where c_1, c_2, c_3 are constants and Φ is the torsional angle. In the TraPPE potential the non-bonded van der Waals interactions are described via a Lennard–Jones 12–6 potential and the cross-alkyl–alkyl interactions (i.e. ε_{ij} and σ_{ij}) are calculated using the Lorenz–Berthelot combining rules (equations (2) and (3)). The parameters used to study the alkyl tether groups in this work are reported in table 2.

In studying alkyl-POSS molecules a number of interactions between the HC and TraPPE force fields must be defined. As in previous work [43], the bond-stretching interactions for Si–CH_3 and Si–CH_2 are approximated by those for Si–C, the angle-bending interactions of O–Si–CH_3 and O–Si–CH_2, are given by O–Si–C, and the torsional interactions for O–Si–CH_2–CH_2 and Si–O–Si–CH_2 are given by X–Si–C–X and Si–O–Si–C, respectively, all from the HC force field. Angle interactions for Si–CH_2–CH_2 and Si–CH_2–CH_3 are approximated by the C–C–C potential in the TraPPE force field, and the torsional interactions for the Si–CH_2–CH_2–CH_2 and Si–CH_2–CH_2–CH_3 bonds are described by the C–C–C–C potential in the TraPPE force field. The parameters for the cross-nonbonded interactions between atoms in the HC and TraPPE force fields are determined following the work of Frischknecht and Curro [50] and are listed in table 3.

Table 1. Parameters used in the HC force field [46, 47] for the POSS systems studied.

Bond	b_0 (Å)	k_2 (kcal/mol Å^2)	k_3 (kcal/mol Å^3)	k_4 (kcal/mol Å^4)
Si–O	1.640	350.1232	−517.3424	673.7067
Si–H	1.478	202.7800	−305.3600	280.2700
Si–C	1.899	189.6500	−279.4200	307.5100
Angle	θ_0 (deg)	H_2 (kcal/mol rad^2)	H_3 (kcal/mol rad^3)	H_4 (kcal/mol rad^4)
Si–O–Si	159.0	8.5000	−13.4188	−4.1785
O–Si–O	110.7	70.3069	−6.9375	0.0000
H–Si–O	107.4	57.6643	−10.6506	4.6274
C–Si–O	114.9	23.0218	−31.3993	24.9814
Dihedral		V_1 (kcal/mol)	V_2 (kcal/mol)	V_3 (kcal/mol)
Si–O–Si–O		−0.225	0.000	−0.010
Si–O–Si–H		0.000	0.000	−0.010
Si–O–Si–C		0.000	0.000	−0.010
Non-bonded interactions			σ_{ij} (Å)	ε_{ij} (kcal/mol)
Si–Si			4.4050	0.19800
Si–Si(C)			4.3494	0.16054
Si–O			4.0323	0.08993
Si–C			4.1744	0.09063
Si(C)–Si(C)			4.2900	0.13100
Si(C)–O			3.9437	0.07710
Si(C)–C			4.1007	0.08560
O–O			3.3000	0.08000
O–C			3.6290	0.06342

Table 2. Parameters used in the TraPPE force field [48] for the alkyl tethers of the POSS systems studied.

Bond		r_{ij} (Å)		k_{ij} (kcal/mol Å^2)
C–C		1.540		889.9
Angle		θ_0 (deg)		k_θ (kcal/mol rad^2)
C–C–C		114.0		124.3122
Dihedral	c_1 (kcal/mol)		c_2 (kcal/mol)	c_3 (kcal/mol)
C–C–C–C	1.4123		−0.27126	3.14786
Non-bonded interactions		σ_{ij} (Å)		ε_{ij} (kcal/mol)
CH_3–CH_3		3.7500		0.194921
CH_3–CH_2		3.8500		0.133544
CH_2–CH_2		3.9500		0.091493

Table 3. Parameters for the cross-nonbonded interactions between atoms in the HC and TraPPE force fields.

Non-bonded interactions	σ_{ij} (Å)	ε_{ij} (kcal/mol)
Si–CH_3	3.830	0.15960
Si–CH_2	3.886	0.10947
O–CH_3	3.380	0.12470
O–CH_2	3.445	0.08550

4. Results

The parameters for POSS in the hetero-SAFT-VR approach were fitted to molecular dynamics simulation data for mono-tethered propyl-POSS at 700 K and 1200 K. The parameters for the alky tethers were taken from earlier work on parameter estimation for the alkanes. In an extensive study of the phase behaviour of *n*-alkanes and their mixtures with the SAFT-VR approach, McCabe and co-workers determined linear relations for the SAFT-VR parameters for the alkane homologous series [25]. These provide simple expressions for the model parameters as a function of molecular weight M_W, namely

$$m\lambda = 0.039M_W + 0.873 \tag{35}$$

$$m\sigma^3 = 1.566M_W + 24.02 \tag{36}$$

$$m(\varepsilon/k) = 6.343M_W + 76.38. \tag{37}$$

The number of segments m in the alkyl chain is determined from the simple relation $m = 1/3(c-1)+1$, as in earlier work [22]. Therefore, in this work only the POSS parameters are optimized. The mono-tethered propyl-POSS system was chosen to determine the POSS parameters rather than hydrogen terminated POSS in order to take into account the effect of the cross-interactions between the POSS and alkyl tether, which are expected to be non-ideal, in an effective way. The parameters obtained from fitting to the PVT data at 700 K and 1200 K for the POSS cube are $\sigma = 6.949$ Å, $\varepsilon/k = 815.5$ K, and $\lambda = 1.8$ and a comparison between the theoretical predictions and simulation data for mono-tethered propyl POSS is shown in figure 2. We note that, particularly at low temperatures, some of the pressures reported are negative which clearly reflects a metastable state.

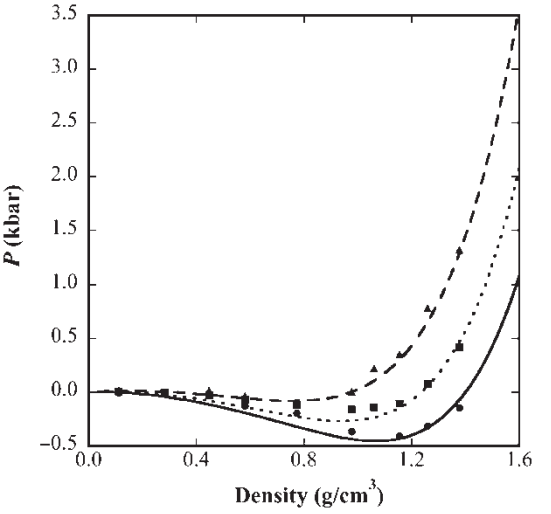

Figure 2. Isotherms for mono-substituted propyl-POSS at 700 K (solid line), 900 K (dotted line), and 1200 K (dashed line). The circles, squares, and triangles represent molecular dynamics simulation results at 700 K, 900 K, and 1200 K respectively.

Once the parameters for the POSS cube were determined, other POSS systems were studied to test parameter transferability. In figure 3 we present the theoretical predictions for mono-tethered hexyl-POSS from the hetero-SAFT-VR approach using the POSS parameters determined from fitting to PVT data for propyl-POSS and alkyl parameters determined using equations (35)–(37). From the figure we can see that

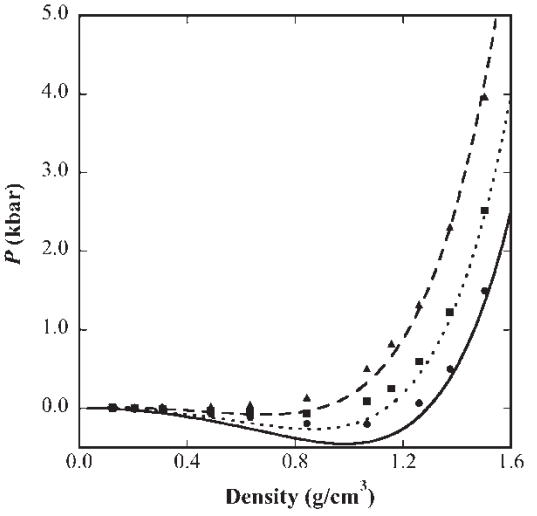

Figure 3. Isotherms for mono-substituted hexyl-POSS at 700 K (solid line), 900 K (dotted line), and 1200 K (dashed line). The circles, squares, and triangles represent molecular dynamics simulation results at 700, 900, and 1200 K, respectively.

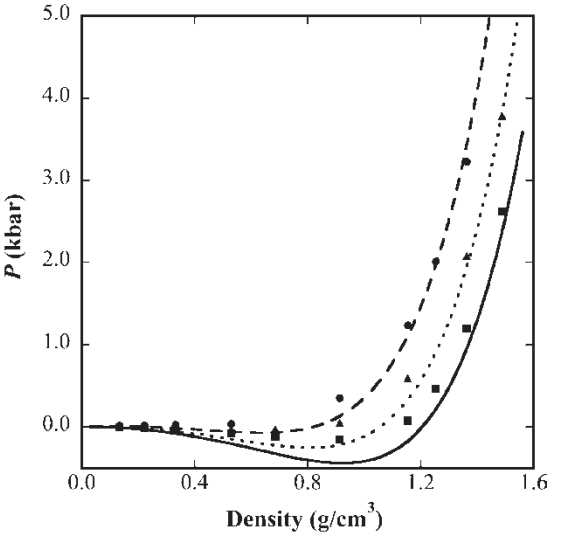

Figure 4. Isotherms for mono-substituted nonyl-POSS at 700 K (solid line), 900 K (dotted line), and 1200 K (dashed line). The circles, squares, and triangles represent molecular dynamics simulation results at 700, 900, and 1200 K, respectively.

the theoretical predictions are in good agreement with the pseudo-experimental data, the deviation between the simulation and theoretical results being less than 10% over the whole isotherm. A similar result is obtained for mono-tethered nonyl-POSS (figure 4), in that good agreement is achieved between the theoretical predictions and the pseudo-experimental data without additional optimization of the parameters. This transferability allows us to predict the behaviour of other

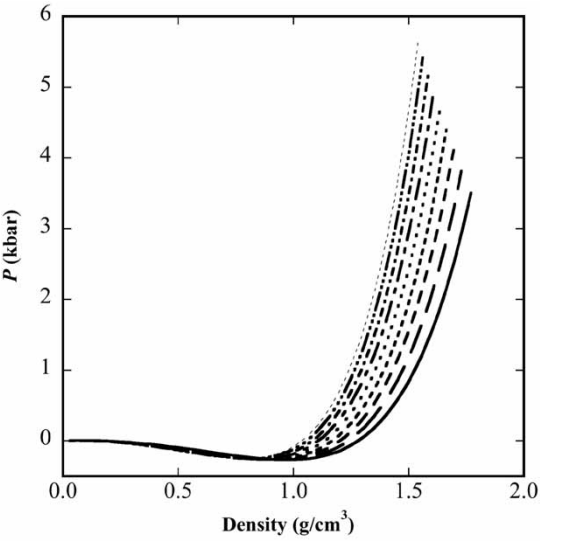

Figure 5. Prediction of isotherms for mono-tethered alkyl-POSS at 900 K. The lines correspond (from right to left) to POSS cubes with ethyl (solid line), propyl, butyl, hexyl, heptyl, octyl, nonyl and decyl tethers.

POSS systems with varying alkyl chain lengths as shown in figure 5 where we consider isotherms at 900 K for tethers from C = 2 to C = 10, respectively. We find that at a given temperature and pressure the liquid density decreases as the tether length increases. This is consistent with the conclusion drawn for the asymmetric diblock model fluids studied in previous work [35], where increasing the fraction of the smaller segments within a molecule resulted in lower densities at a given pressure and temperature.

We have also studied the effect of the number of tethers on the thermodynamic properties of multi-tethered POSS systems. Figure 6 presents theoretical predictions for isotherms at 700 K, 900 K, 1200 K for di-tethered propyl-POSS. From the figure we note that while there is good agreement between the theoretical predictions and simulation data at 1200 K, deviations are observed at low pressures for the other temperatures studied. We have also calculated isotherms for tetra-tethered propyl-POSS with two different arrangements of the tethers on the POSS cube; tetra-tethered propyl-POSS with the tethers on one face of the cube (figure 1(d)) and tetra-tethered propyl-POSS with the tethers on opposite corners of the cube (figure 1(e)). We find from the simulation results (as shown in figure 7) that the differences between the two systems are very small, and therefore a comparison with the hetero-SAFT-VR predictions, which cannot distinguish between the different arrangements of the tethers on the POSS cube, is reasonable. However, we find that while the agreement between the theory and simulation is good at low denstities, the density is underpredicted at

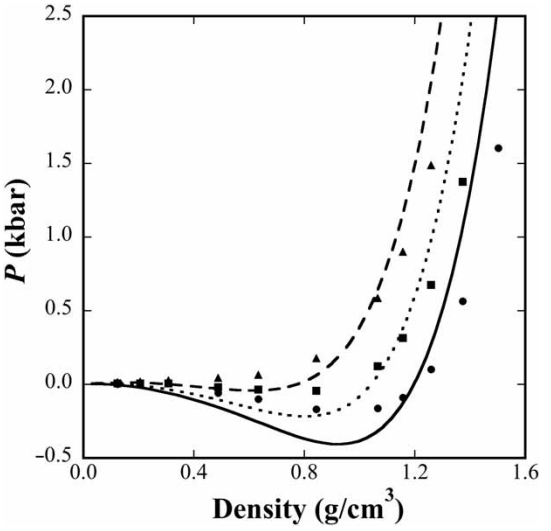

Figure 6. Isotherms for di-tethered propyl-POSS at 700 K (solid line), 900 K (dotted line), and 1200 K (dashed line). The circles, squares, and triangles represent molecular dynamics simulation results at 700, 900, and 1200 K, respectively.

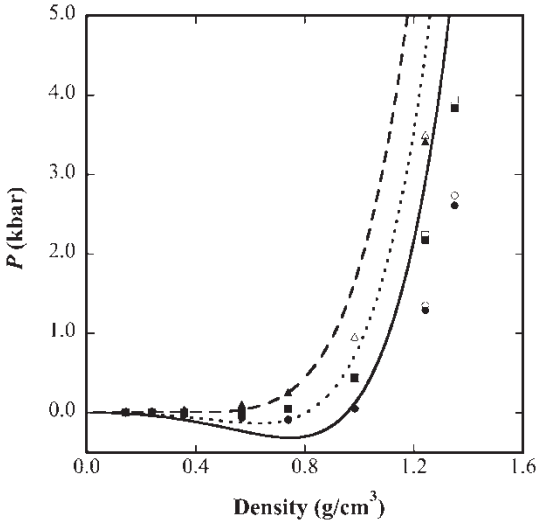

Figure 7. Isotherms for tetra-tethered propyl-POSS at 700 K (solid line), 900 K (dotted line), and 1200 K (dashed line). The circles, squares, and triangles represent molecular dynamics simulation results at 700, 900, and 1200 K, respectively. Empty symbols are for the configuration in figure 1(d) and solid for the configuration in figure 1(e).

a given temperature and pressure for higher densities ($>0.8\,g/cm^3$). Finally, results for octa-tethered propyl-POSS are presented in figure 8. From figures 6, 7, and 8, we can see that the deviation between the theoretical prediction and the simulation data increases as the number of tethers increases. This deviation may be caused by the fact that the tethers on the POSS cage in the hetero-SAFT-VR approach are fully flexible and

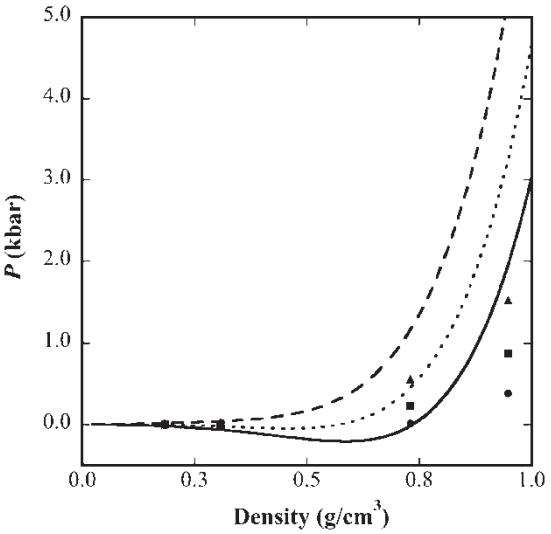

Figure 8. Isotherms for octa-tethered propyl-POSS at 700 K (solid line), 900 K (dotted line), and 1200 K (dashed line). The circles, squares, and triangles represent molecular dynamics simulation results at 700, 900, and 1200 K, respectively.

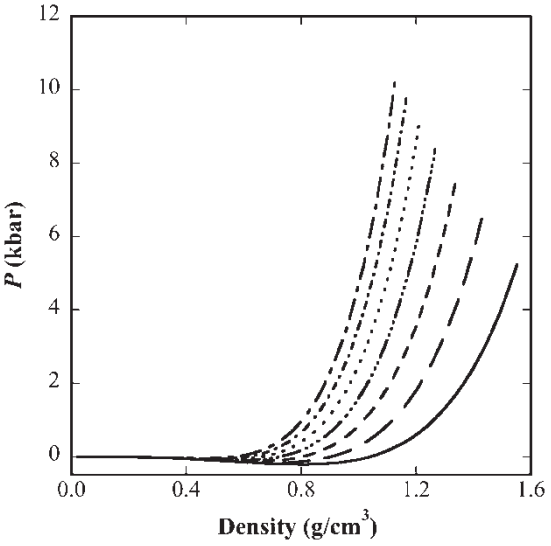

Figure 9. Prediction of isotherms for multi-tethered propyl-POSS at 900 K. The lines correspond to POSS cubes with 2 (solid line), 3, 4, 5, 6, and 8 tethers (from right to left).

their arrangement cannot be specified as in the MD simulations, and so perhaps steric effects are not accurately captured.

In order to gain some insight into the effect of the number of tethers on the thermodynamic properties, isotherms at 900 K for a series of multi-propyl-substituted POSS systems with the number of tethers varying from 2 to 8 were calculated and the results are presented in figure 9. We find that as the number of tethers increases the density decreases at a given

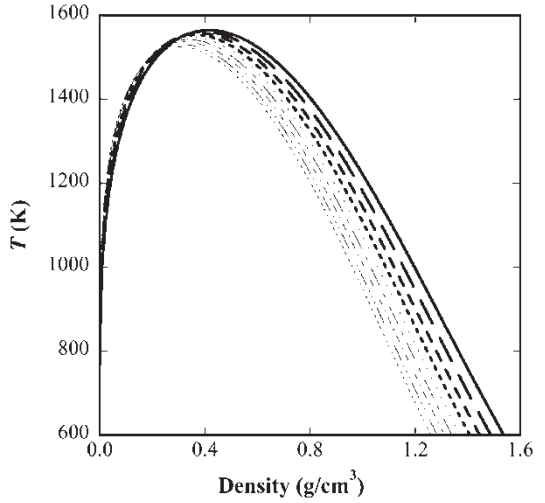

Figure 10. Prediction of vapour–liquid equilibrium curves for mono-tethered alkyl-POSS. The lines correspond to POSS cubes with ethyl (solid line), propyl, butyl, hexyl, heptyl, octyl, nonyl and decyl tethers (from right to left).

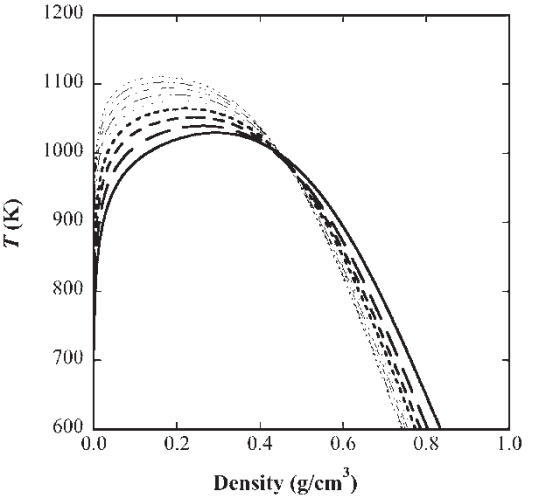

Figure 11. Prediction of vapour–liquid equilibrium curves for octa-tethered alkyl-POSS. The lines correspond to POSS cubes with ethyl (solid line), propyl, butyl, hexyl, heptyl, octyl, nonyl and decyl tethers (from right to left).

Table 4. Model fluid systems studied and predicted trends in T_c as a function of tether length.

System	m_1	m_2	σ_2/σ_1	$\varepsilon_2/\varepsilon_1$	λ_1	λ_2	T_c
1	$1 \rightarrow 10$	1	1.6	3	1.5	1.5	$\downarrow$
2	$1 \rightarrow 10$	1	1.6	3	1.5	1.8	$\downarrow$
3	$1 \rightarrow 10$	1	1.8	3	1.5	1.8	$\downarrow$
4	$1 \rightarrow 10$	1	1.8	3	1.8	1.8	$\uparrow\downarrow$
5	$1 \rightarrow 10$	1	1.8	4	1.5	1.8	$\downarrow$
6	$1 \rightarrow 10$	1	1.8	4	1.8	1.8	$\downarrow$
7	$1 \rightarrow 10$	1	2	3	1.5	1.8	$\downarrow$
8	$1 \rightarrow 10$	1	2	3	1.8	1.8	$\uparrow\downarrow$

temperature and pressure, which is in agreement with the MD simulation results for tetra-substituted POSS compared to octa-substituted POSS.

We have also studied the vapour–liquid equilibrium (VLE) of a series of mono-substituted alkyl-POSS systems, the results of which are presented in figure 10. From the calculations we find that the critical temperature decreases as the length of the tether increases, which is consistent with the tethers disrupting the packing and interaction of the POSS cubes.

Since the POSS parameters used in this work were determined by fitting to limited pseudo-experimental data we have also studied a number of model fluids in order to obtain a better understanding of the effect of the parameters on the observed properties and trends. Each model fluid studied mimics a mono-tethered POSS system in that it is composed of two types of segments that have different size and energy parameters, with the number of smaller segments ranging from 1 to 10. The systems studied are listed in table 4 along with the observed trend in the critical temperature as the tether length is increased from 1 to 10. We find that generally the critical temperature decreases as the number of tether segments increases. Therefore, we expect the predictions from the hetero-SAFT-VR approach for mono-tethered alkyl-POSS to be at least qualitatively accurate.

Finally, the VLE curves for a series of octa-substituted alkyl-POSS systems of varying tether length have also been studied and are presented in figure 11. For octa-tethered POSS we find that the VLE curves intersect at a density of $\sim 0.5\,\mathrm{g/cm^3}$ and the predicted critical points increase with increasing tether length. Experimentally, the critical points of the *n*-alkanes also increases with carbon number. Furthermore, it is well known that while the melting points of the alkanes increases with carbon number, for relatively short chains an odd-*n*/even-*n* behaviour is observed (the alternation becomes attenuated with increasing carbon number and is not detectable for $n > 16$) [51] and a plot of critical temperature versus melting point indicates a strong correlation or cooperative phenomena between the two properties [5]. The melting points of octa-substituted alkyl-POSS first decreases from C_3 to C_5 and then increases gently from C_5 to C_{10}, with octa-tethered propyl-POSS having the highest melting point of the systems studied and an odd–even effect being observed for C_5–C_{10}, which was the longest alkyl chain tether studied [4]. The decrease in

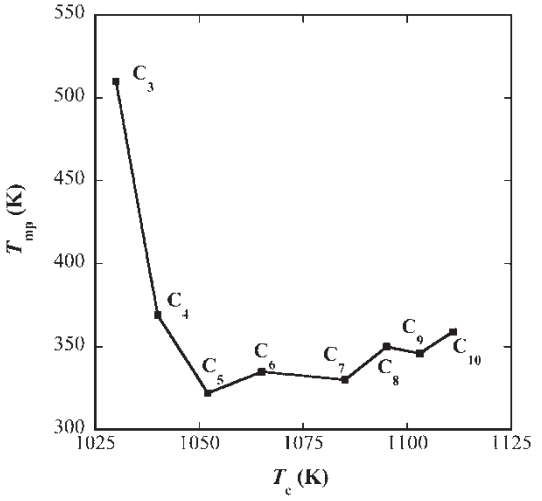

Figure 12. Experimental melting points versus critical temperature for octa-substituted alkyl-POSS of increasing chain length from C_3–C_{10} predicted from the hetero-SAFT-VR EOS.

melting point from C_3 to C_5 is presumably due to the dominant effect of the POSS cube, which diminishes as the chain length of the alkyl tether increases. The predicted critical points for octa-substituted alkyl-POSS when plotted against their experimental melting points as in figure 12, appear to follow a similar linear trend and could enable the melting points of octa-substituted alkyl-POSS molecules with longer tether lengths to be determined from the hetero-SAFT-VR predictions for the critical temperature.

5. Conclusions

The hetero-SAFT-VR approach has been applied to study alkyl-substituted POSS fluids. Atomistic molecular dynamics simulations were performed for three mono-tethered POSS systems and four multi-tethered POSS systems, and in general good agreement obtained between the theoretical predictions and the simulation data. We find that as the length of the alkyl tether increases, the liquid density of mono-substituted POSS systems decreases at a given temperature and pressure. Additionally, for multi-substituted POSS systems, the density was seen to decrease as the number of tethers increased at a given temperature and pressure. For the tetra- and octa-substituted POSS systems studied, deviations were observed between the simulation data and theoretical predictions, which could be due to steric effects that are not captured by the hetero-SAFT-VR approach due to the fully flexible nature of the molecules depicted by the model. However, we note that the results for the multi-tethered POSS systems can be considered reasonable since the hetero-SAFT-VR parameters for the POSS cube were obtained by fitting to PVT data for mono-tethered propyl-POSS and no binary interaction parameter between the POSS group and alkyl groups were used to take into account the dissimilarity of the POSS and alkyl segments. The phase behaviour of the POSS systems studied was also investigated and the critical points predicted as a function of tether length and the number of tethers on the POSS cube. For mono-substituted alkyl-POSS, the critical temperature is predicted to decrease with increasing tether length from C_3 to C_{10}, while for octa-substituted alkyl-POSS systems the critical temperature increases as tether length increases from C_3 to C_{10}. Furthermore, experimental melting points versus predicted critical temperatures for octa-tethered alkyl-POSS systems were found to exhibit a linear-like trend as the tether length increased from C_5 to C_{10}, as is seen for the *n*-alkanes.

Acknowledgments

We acknowledge support from the National Science Foundation through grant number DMR-0103399 and our collaborators on the NIRT project. In particular, we thank Shannon Capps, Tudor Ionescu, and Patrick Redmill for useful discussions.

References

[1] R. M. Laine, J. Mater. Chem. **15,** 3725 (2005).
[2] B. X. Fu, L. Yang, R. H. Somani, S. X. Zong, B. S. Hsiao, S. Phillips, R. Blanski, and P. Ruth, J. Polym. Sci. Pt. B-Polym. Phys. **39,** 2727 (2001).
[3] E. T. Kopesky, T. S. Haddad, R. E. Cohen, and G. H. McKinley, Macromolecules **37,** 8992 (2004).
[4] C. Bolln, A. Tsuchida, H. Frey, and R. Mulhaupt, Chem. Mater. **9,** 1475 (1997).
[5] A. T. Balaban, D. J. Klein, N. H. March, M. P. Tosi, and M. Ausloos, Chem. Phys. Chem. **6,** 1741 (2005).
[6] R. Knischka, F. Dietsche, R. Hanselmann, H. Frey, R. Mulhaupt, and P. J. Lutz, Langmuir **15,** 4752 (1999).
[7] R. K. Bharadwaj, R. J. Berry, and B. L. Farmer, Polymer **41,** 7209 (2000).
[8] M. H. Lamm, T. Chen, and S. C. Glotzer, Nano Lett. **3,** 989 (2003).
[9] Y. J. Sheng, W. J. Lin, and W. C. Chen, J. Chem. Phys. **121,** 9693 (2004).
[10] F. M. Capaldi, G. C. Rutledge, and M. C. Boyce, Macromolecules **38,** 6700 (2005).
[11] A. Striolo, C. McCabe, and P. T. Cummings, J. Phys. Chem. B **109,** 14300 (2005).
[12] A. Striolo, C. McCabe, and P. T. Cummings, Macromolecules **38,** 8950 (2005).
[13] R. R. Patel, R. Mohanraj, and C. U. Pittman, J. Polym. Sci. B-Polym. Phys. **44,** 234 (2006).

[14] X. Zhang, E. R. Chan, and S. C. Glotzer, J. Chem. Phys. **123**(18)**,** (2005).
[15] H.-C. Li, C. McCabe, A. Striolo, and P. T. Cummings, J. Phys. Chem. B (submitted).
[16] A. Striolo, C. McCabe, and P. T. Cummings, J. Chem. Phys. **125**(10)**,** (2006).
[17] A. Striolo, E. R. Chan, C. McCabe, S. C. Glotzer, and P. T. Cummings, J. Phys. Chem. B submitted (2006).
[18] W. G. Chapman, G. Jackson, and K. E. Gubbins, Mol. Phys. **65,** 1057 (1988).
[19] W. G. Chapman, K. E. Gubbins, G. Jackson, and M. Radosz, Ind. Eng. Chem. Res. **29,** 1709 (1990).
[20] E. A. Muller and K. E. Gubbins, in *Equations of State for Fluids and Fluid Mixtures*, edited by J. V. Sengers, R. F. Kayser, C. J. Peters, and H. J. J. White (Elsevier, Amsterdam, 2000), Vol. I, p. 435.
[21] I. G. Economou, Ind. Eng. Chem. Res. **41,** 953 (2002).
[22] A. Gil Villegas, A. Galindo, P. J. Whitehead, S. J. Mills, G. Jackson, and A. N. Burgess, J. Chem. Phys. **106,** 4168 (1997).
[23] A. Galindo, L. A. Davies, A. Gil-Villegas, and G. Jackson, Mol. Phys. **93,** 241 (1998).
[24] C. McCabe, A. Gil-Villegas, and G. Jackson, J. Phys. Chem. B **102,** 4183 (1998).
[25] C. McCabe and G. Jackson, PCCP Phys. Chem. Chem. Phys. **1,** 2057 (1999).
[26] C. McCabe, A. Galindo, M. N. Garcia-Lisbona, and G. Jackson, Ind. Eng. Chem. Res. **40,** 3835 (2001).
[27] A. Galindo, A. Gil-Villegas, G. Jackson, and A. N. Burgess, J. Phys. Chem. B **103,** 10272 (1999).
[28] A. Gil-Villegas, A. Galindo, and G. Jackson, Mol. Phys. **99,** 531 (2001).
[29] B. H. Patel, P. Paricaud, A. Galindo, and G. C. Maitland, Ind. Eng. Chem. Res. **42,** 3809 (2003).
[30] C. McCabe and S. B. Kiselev, Fluid Phase Equilib. **219,** 3 (2004).
[31] L. X. Sun, H. G. Zhao, S. B. Kiselev, and C. McCabe, Fluid Phase Equilib. **228,** 275 (2005).
[32] L. X. Sun, H. G. Zhao, S. B. Kiselev, and C. McCabe, J. Phys. Chem. B **109,** 9047 (2005).
[33] H. G. Zhao and C. McCabe, J. Chem. Phys. **125**(10)**,** (2006).
[34] C. McCabe, A. Gil-Villegas, G. Jackson, and F. Del Rio, Mol. Phys. **97,** 551 (1999).
[35] Y. Peng, H. G. Zhao, and C. McCabe, Mol. Phys. **104,** 571 (2006).
[36] J. S. Rowlinson and F. L. Swinton, *Liquids and Liquid Mixtures*, 3rd ed. (Butterworth Scientific, London, 1982).
[37] P. J. Leonard, D. Henderso, and J. A. Barker, Trans. Faraday Soc. **66,** 2439 (1970).
[38] T. Boublik, J. Chem. Phys. **53,** 471 (1970).
[39] G. A. Mansoori, N. F. Carnahan, K. E. Starling, and T. W. Leland, J. Chem. Phys. **54,** 1523 (1971).
[40] N. F. Carnahan and K. E. Starling, J. Chem. Phys. **51,** 635 (1969).
[41] W. Smith and T. R. Forester, J. Mol. Graph. **14,** 136 (1996).
[42] H. J. C. Berendsen, J. P. M. Postma, W. F. Vangunsteren, A. Dinola, and J. R. Haak, J. Chem. Phys. **81,** 3684 (1984).
[43] T. C. Ionescu, F. Qi, C. McCabe, A. Striolo, J. Kieffer, and P. T. Cummings, J. Phys. Chem. B **110,** 2502 (2006).
[44] M. G. Voronkov and V. I. Lavrentyev, Topics Current Chem. **102,** 199 (1982).
[45] J. I. Siepmann, S. Karaborni, and B. Smit, Nature **365,** 330 (1993).
[46] H. Sun, Macromolecules **28,** 701 (1995).
[47] H. Sun and D. Rigby, Spectrosc. Acta A-Mol. Biomol. Spectrosc. **53,** 1301 (1997).
[48] M. G. Martin and J. I. Siepmann, J. Phys. Chem. B **102,** 2569 (1998).
[49] H.-C. Li, C.-Y. Lee, C. McCabe, A. Striolo, and M. N. Neurock, J. Phys. Chem. A submitted (2006).
[50] A. L. Frischknecht and J. G. Curro, Macromolecules **36,** 2122 (2003).
[51] R. Boese, H. C. Weiss, and D. Blaser, Angew. Chem.- Int. Edn **38,** 988 (1999).